Journal of Magnetic Resonance **153,** 124–132 (2001)
doi:10.1006/jmre.2001.2436, available online at http://www.idealibrary.com on IDEAL®

Improved Resolution Using Symmetrically Shifted Pulses

Krish Krishnamurthy

Discovery Chemistry Research, Lilly Research Laboratories, Indianapolis, Indiana 45285

Received June 4, 2001; revised August 10, 2001; published online October 5, 2001

An approach to Hadamard phase encode the two halves of the F_1 dimension of a gHSQC experiment is presented. The phase encoding is achieved by excitation sculpting of the F_1 dimension using symmetrically shifted pulses. This approach (IMPRESS—improved resolution using symmetrically shifted pulses) increases the resolution of the F_1 dimension by exploiting spectral folding, but the folding is coded in the fashion of a Hadamard H_2 matrix. Editing of the IMPRESS spectra during processing sorts out spectral crowding which is a typical consequence of F_1 spectral folding. It is shown that for the same total experiment time, the IMPRESS-gHSQC experiment provides narrower peaks along the F_1 dimension compared to the normal gHSQC experiment. As a consequence of decreased linewidth, the peak height (sensitivity) is also increased.

Key Words: **excitation sculpting; HSQC; band-selective excitation; DPFGSE; spectral editing; spectral folding.**

INTRODUCTION

Band-selective pulses have been used in multidimensional NMR to select a desired spectral region in one or more dimensions (*1–8*). The reduction of the spectral width in one or more dimensions improves the digital resolution achievable in the chosen dimension and reduces ambiguities in the resonance assignment procedure in a crowded spectral region. The reduction in the evolution spectral width also shortens the measurement time of the experiment. The recent report (*9*) on the use of excitation sculpting and PFGSE in band-selective HSQC and HMBC experiment exploits this approach to increase the F_1 resolution. The obvious drawback of region-selective experiments is that multiple acquisitions must be performed to generate spectra of different regions.

Another approach is to exploit spectral folding along F_1. In this approach the indirect dimension spectral width is kept to one-half or one-third of the "required" width, thus allowing the peaks outside the Nyquest frequency to fold in. This approach typically relies on the phase(s) of the observed resonances or patterns to sort out the spectral crowding (*10*). We now wish to report an IMPRESS-HSQC (improved resolution using symmetrically shifted pulses) experiment which uses the Hadamard excitation sculpting technique. This approach also exploits spectral folding to improve F_1 resolution (or decrease total measuring time) but the folding is coded in the fashion of a Hadamard H_2 matrix (*11–14*). This provides a way to edit the spectra during processing to sort out spectral crowding, which is a typical consequence of data sampling at a rate slower than that dictated by the Nyquest theorem.

RESULTS AND DISCUSSION

Excitation sculpting (*15*) is produced by the application of a double pulse field gradient spin-echo sequence (DPFGSE) as shown in Fig. 1A. Excitation sculpting associates very clean frequency selection with "user-friendliness" and hence has recently enjoyed undeniable success both in frequency-selective 1D experiments such as NOESY1D and in band-selected 2D experiments (*8, 9, 16–19*). In typical applications of excitation sculpting the two selective pulses (S_1 and S_2) are kept the same. However, this need not be the case. For example, in a two-site excitation sculpting we recently showed (*20*) that "*in-phase*" or "*anti-phase*" echoes for the selected frequencies could be generated by the appropriate selection of S_1 and S_2 waveforms. If S_1 and S_2 are set to S_{xx} (where S_{xx} is a double-frequency shifted waveform which effects the refocusing RF event about the x-axis for both frequency positions) one generates in-phase echoes for the two frequencies. Alternately, if $S_1 = S_{xx}$ and $S_2 = S_{xy}$ (where S_{xy} is same as S_{xx} except that the refocusing RF event is about the x-axis for the first frequency and about the y-axis for the second frequency) one generates anti-phase echoes for the two frequencies. The two shapes, S_{xx} and S_{xy} are double-frequency shifted laminar pulses (*21*) and differ only in the relative phase of the two phase ramps. In the former case the nominal phase (*22*) is the same for both phase ramps, while in the latter they are quadrature shifted. Two spectra generated in this fashion ($S_1 = S_2 = S_{xx}$ and $S_1 = S_{xx}$; $S_2 = S_{xy}$) can be viewed as the components of a Hadamard H_2 matrix. The two selected resonances can then be sorted out by appropriate linear combination. It was previously shown (*20*) that such Hadamard excitation (HEX) sculpting can significantly improve sensitivity and/or decrease the total experiment time over excitation sculpting performed one frequency at a time.

HEX sculpting is applicable to wideband excitation as well. Figure 2 represents experimental excitation profiles using the DPFGSE train and "constant-adiabaticity" WURST (*23–25*) 180° pulses. For the profile in Fig. 2a, S_1 and S_2 are set to an

1090-7807/01 $35.00

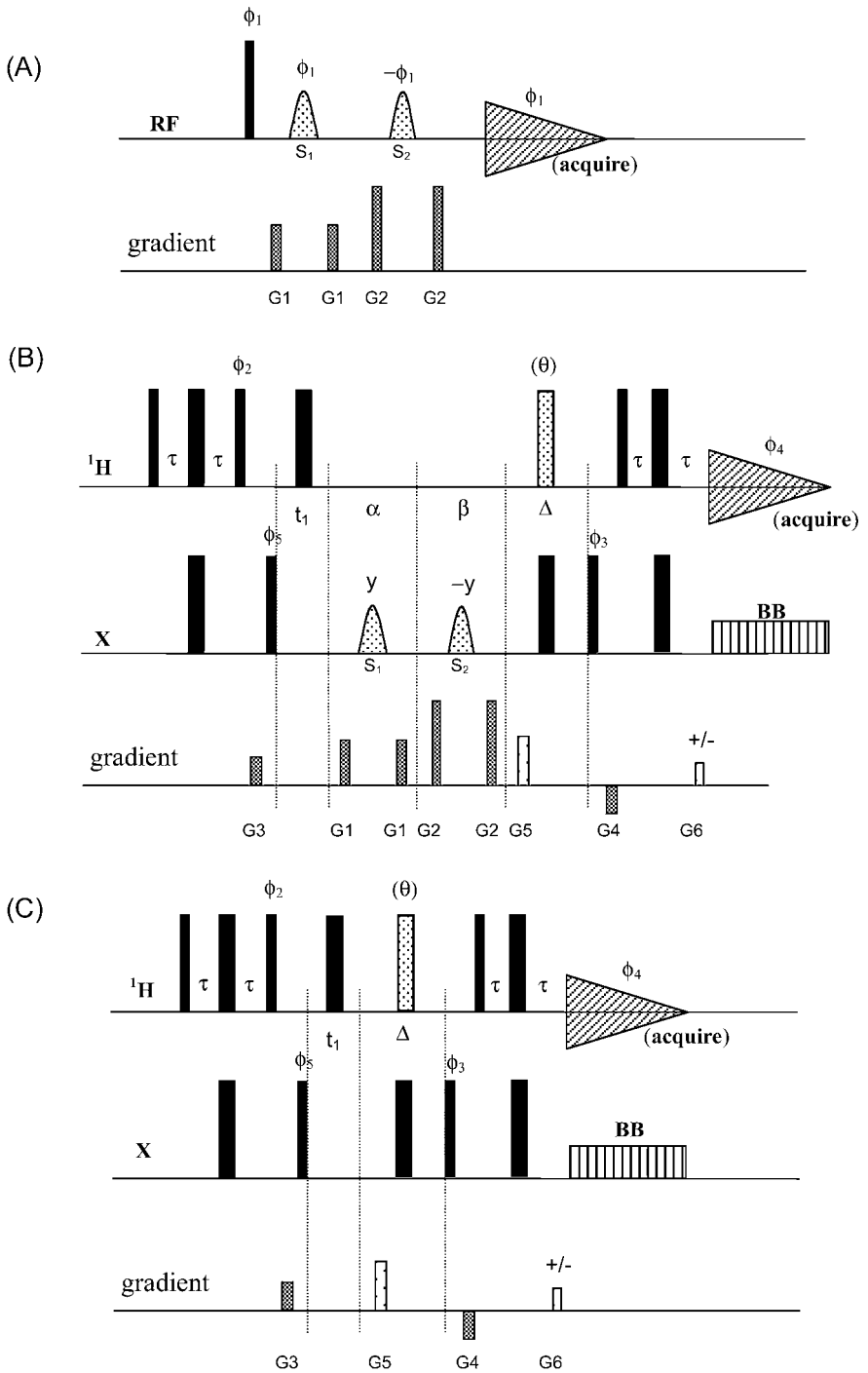

FIG. 1. Pulse sequences for (A) the double PFG spin-echo; (B) IMPRESS-gHSQC; and (C) gHSQC. Thin and thick vertical lines represents 90° and 180° pulses. The band-selective pulses (S_1 and S_2) are 180° pulses. The delay τ is set to $1/4J$. The delays α and β (and the PFG echo times in sequence A) are set to minimum values to accommodate the gradient pulses, the band-selective pulses, and gradient recovery delays. The pulse angle θ is set to either 0° pulse (no CH multiplicity editing) or 180° (CH multiplicity editing). The delay Δ is set to either $1/J$ ($\theta = 180°$ pulse) or a minimum value to accommodate the gradient and RF pulses. The basic phase cycling is $\phi_1 = x$; $\phi_2 = y, y, -y, -y$; $\phi_3 = x, x, x, x, -x, -x, -x, -x$; $\phi_4 = x, -x, -x, x, -x, x, x, -x$; $\phi_5 = x, -x$. Phases not shown are along the x axis. The gradients G5 and G6 are set in the ratio 1 : 3.98 for CH coherence selection. Pure N- and P-type data are collected by inverting the sign of the G6 gradient, stored separately, and combined during processing to generate pure absorptive lineshapes. The gradient amplitudes are set to G1 : G2 : G3 : G4 : G5 : G6 = 2 : 10 : 10 : 6 : 10 : 2*G5/3.98 G/cm while the durations are set to G1 : G2 : G3 : G4 : G5 : G6 = 0.5 : 0.5 : 10 : 6 : 2 : 1 ms.

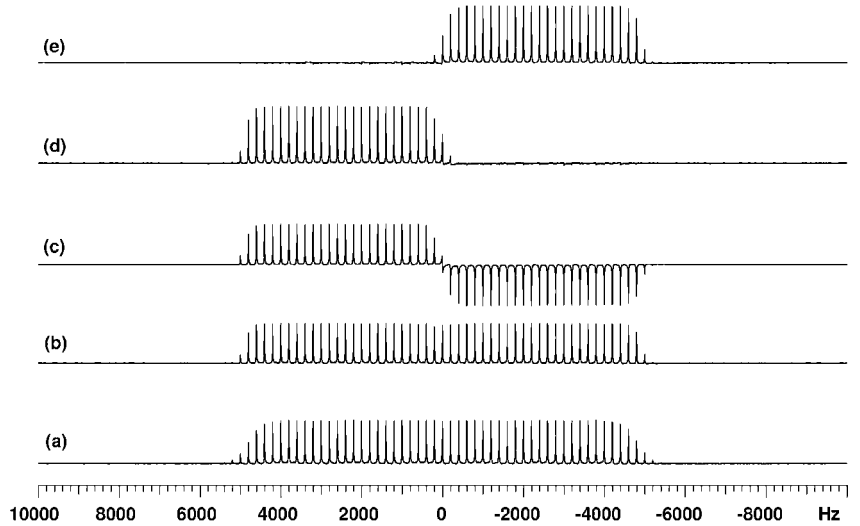

FIG. 2. Single and double frequency selected profiles using DPFGSE. (a) Using a 8-ms caWURST pulse ($B_{1(\mathrm{rms})} = 0.893$ kHz) to achieve 10-kHz bandwidth refocusing; $S_1 = S_2$; (b) Using a 16-ms caWURST pulse ($B_{1(\mathrm{rms})} = 0.631$ kHz) to achieve 5-kHz bandwidth refocusings at $+/-2.5$-kHz frequency offsets. $S_1 = S_2 = S_{xx}$, where S_{xx} represents that the nominal phase of the two waveforms are in-phase; (c) Using a 16-ms caWURST pulse ($B_{1(\mathrm{rms})} = 0.631$ kHz) to achieve 5-kHz bandwidth refocusings at $+/-2.5$-kHz frequency offsets. $S_1 = S_{xx}$ and $S_2 = S_{xy}$, where S_{xy} represents that the nominal phase of the two waveforms are orthogonal with respect to each other; (d) Sum of the profiles in b and c; (e) Difference of the profiles in b and c. The profiles are plotted with the vertical scaling factor adjusted to have same noise levels.

on-resonance caWURST pulse for a 10-kHz bandwidth refocusing. The profiles in Figs. 2b and 2c are for two-site HEX sculpting. For the profile in Fig. 2b S_1 and S_2 are set to the S_{xx} pulse, while for Fig. 2c, S_1 is set to S_{xx} and S_2 is set to S_{xy}. The S_{xx} and S_{xy} pulses are a linear combination of two caWURST off-resonance (frequency offsets set to $+/-2.5$ kHz and bandwidth of refocusing set to 5 kHz each) shapes with their nominal phases being x,x or x,y, respectively. The excitation profile in Fig. 2b is very similar to that in Fig. 2a, except for a small "notch" in the center of the profile. The profile in Fig. 2c is very similar to that in Fig. 2b except for the relative phase of the two bands. The two bands in Figs. 2b and 2c can be edited (add or subtract) to generate the individual band profiles as shown in Figs. 2d and 2e. The S/N improvement in these bands is expected to be the square root of 2 over similar profiles generated one at time.

We applied this HEX editing to the carbon dimension of a gradient HSQC experiment. The IMPRESS-gHSQC sequence is shown in Fig. 1B along with the standard gHSQC sequence (Fig. 1C). The IMPRESS-gHSQC sequence is similar to gHSQC experiment except that a DPFGSE pulse train now follows the evolution period. This pulse sequence is very similar to the one reported by Nuzillard and co-workers (*9*) for band-selective HSQC. If S_1 and S_2 are set to select a particular ^{13}C chemical bandwidth, then one observes only those carbons that are in the selected region. This allows one to reduce the spectral width in the indirect dimension and improve resolution and/or sensitivity. Alternately, such band selection allows one to reduce the number of t_1 increments (and hence the total experiment time) to be collected to achieve a target resolution along the ^{13}C dimension. This is illustrated in the comparison of a gHSQC spectrum with band-selected gHSQC spectra of strychnine in Fig. 3. The band-selective spectra (Figs. 3b and 3c) were obtained using sequence 1B. The S_1 and S_2 shapes are caWURST refocusing pulses to achieve 71 ppm (8.9-kHz ^{13}C chemical shift in a 500-MHz spectrometer) band selection. For the spectrum in Fig. 3b the ^{13}C pulses were centered at 106.5 ppm while for the spectrum in Fig. 3c it was centered at 35.5 ppm. The nonselective spectrum in Fig. 3a was obtained using sequence 1C. The number of t_1 increments is the same in all three cases, but the ^{13}C spectral width in the band-selective spectra is only half that in the nonselective spectrum. As expected (in the F_1 projections), the resolution along the ^{13}C dimension is twice in the band-selective experiments compared to the nonselective experiment. However, doing two band-selective experiments to achieve higher resolution for all ^{13}C cross peaks is no different (in terms of time saving) than running the nonselective experiment with twice the number of t_1 increments. The IMPRESS-gHSQC achieves this desired higher resolution without increasing the total experimental time by using Hadamard excitation sculpting.

In Fig. 4, "unedited" IMPRESS-gHSQC spectra of a sample of Taxol are shown. Both spectra were collected, each with a 90-ppm ^{13}C spectral width, 180 t_1 increments, and four scans per increment. The spectrum in Fig. 4a was collected with $S_1 = S_2 = S_{xx}$ while that in Fig. 4b was collected with $S_1 = S_{xx}$ and $S_2 = S_{xy}$. The shapes S_{xx} and S_{xy} are dual band (9 kHz each), symmetrically shifted ($+/-4.5$ kHz) laminar caWURST refocusing pulses. The two shapes differ only in the nominal phase of the $(+)$4.5-kHz frequency (downfield with respect to carrier frequency) shifted waveform and the $(-)$4.5-kHz frequency

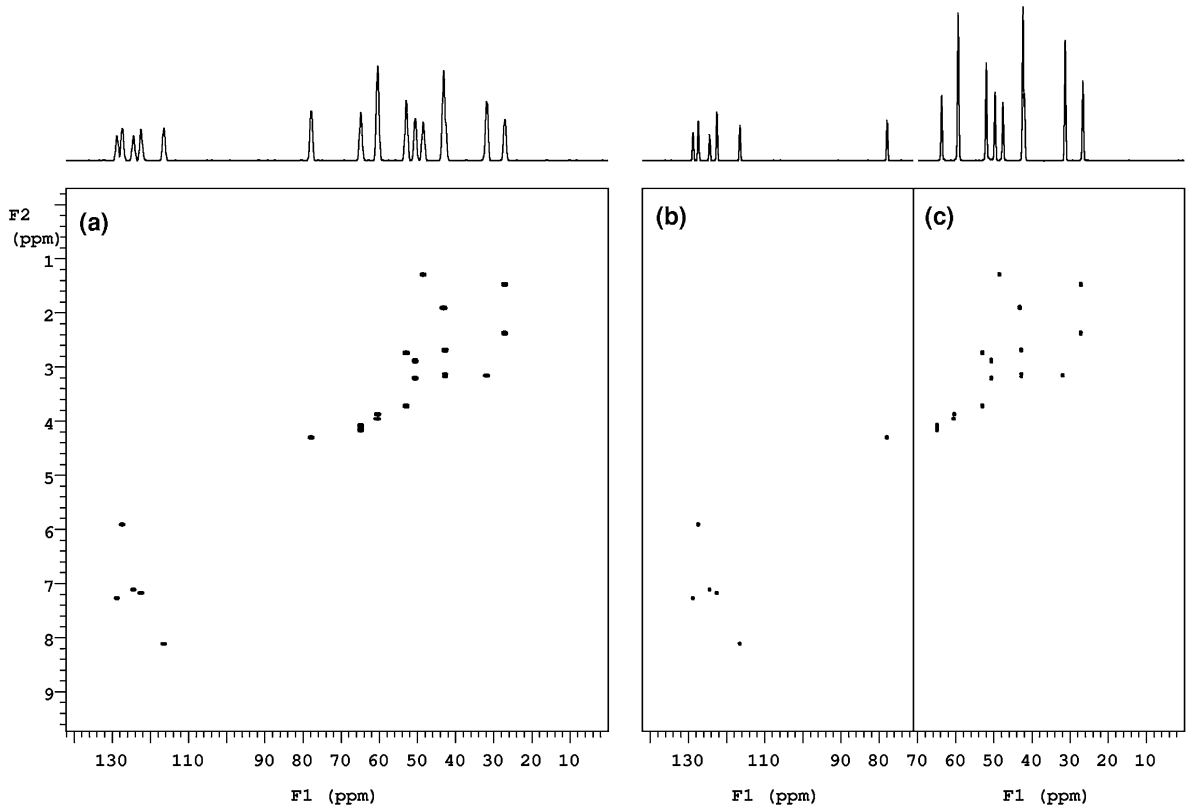

FIG. 3. Comparison of a nonselective gHSQC and band-selective gHSQC of a sample of strychnine in CDCl3. The nonselective spectrum (a) is obtained using the sequence in Fig. 1C and the band-selective spectra (b and c) use the sequence in Fig. 1B.

(upfield with respect to carrier frequency) shifted waveform. While in the S_{xx} shape the two waveforms have the same phase (x and x), in the S_{xy} shape the two waveforms have orthogonal phase (x and y). The spectra were processed with $(-)$4.5-kHz frequency shift (difference between the carrier frequency and the center of the upfield band) applied to the t_1 interferograms prior to transformation. This results in the peaks within the upfield band (9-kHz band centered at $(-)$4.5 kHz from the carrier) to appear "as is" and the peaks within the downfield band (9-kHz band centered at $(+)$4.5 kHz from the carrier) to fold over with sign inversion. The spectrum in Fig. 4b has all the frequencies in phase (although the downfield set, i.e., the 9-kHz band centered at $(+)$4.5 kHz from the carrier, is sign inverted due to foldover) and the spectrum in Fig. 4a has the upfield set anti-phase with respect to the downfield set.

The two spectra in Fig. 4 represent elements of a Hadamard H_2 matrix and can be sorted out by appropriate linear combination. The spectrum in Fig. 5a is the edited IMPRESS-gHSQC spectrum with the downfield and upfield halves plotted side by side. This spectrum was obtained from the two datasets shown in Fig. 4, by addition (downfield half) and subtraction (upfield half). It is compared to a standard gHSQC spectrum (Fig. 5b) obtained using 180-ppm ^{13}C spectral width, 180 t_1 increments, and eight scans per increment. The total experiment time (1 h) for the gHSQC experiment is same as the sum of the experiment times for the two IMPRESS-gHSQC spectra (30 min each).

The improved resolution in IMPRESS-gHSQC experiment over a gHSQC experiment is clearly evident in the expansions and projections presented in Fig. 6. In Figs. 6a and 6b expanded regions and ^{13}C projections from the gHSQC and IMPRESS-gHSQC are shown. These expansions and projections were plotted with the vertical scaling factor adjusted such that the average (from four F_2 traces with no cross peaks) measured noise is the same in both spectra. The IMPRESS-gHSQC cross peaks clearly have higher resolution over the corresponding gHSQC cross peaks as evidenced in both the 2D contours and the F_1 projection. The increased signal height is undoubtedly coming from the narrowing of the peak widths. One would anticipate a signal loss in IMPRESS-gHSQC due to ^{13}C relaxation during the relatively long band-selective pulses. The signal height increase (and hence S/N in its traditional definition) due to line narrowing more than compensates for this relaxation loses. The sensitivity increase due to line narrowing is also evidenced in the F_2 skyline projections shown in Figs. 6c and 6d. These projections are plotted with the vertical scaling factor adjusted to the same noise level to enable the direct comparison of the signal height as a measure of S/N. A 1-ppm expansion ($10\times$ vertical expansion) of the noise is also plotted for comparison.

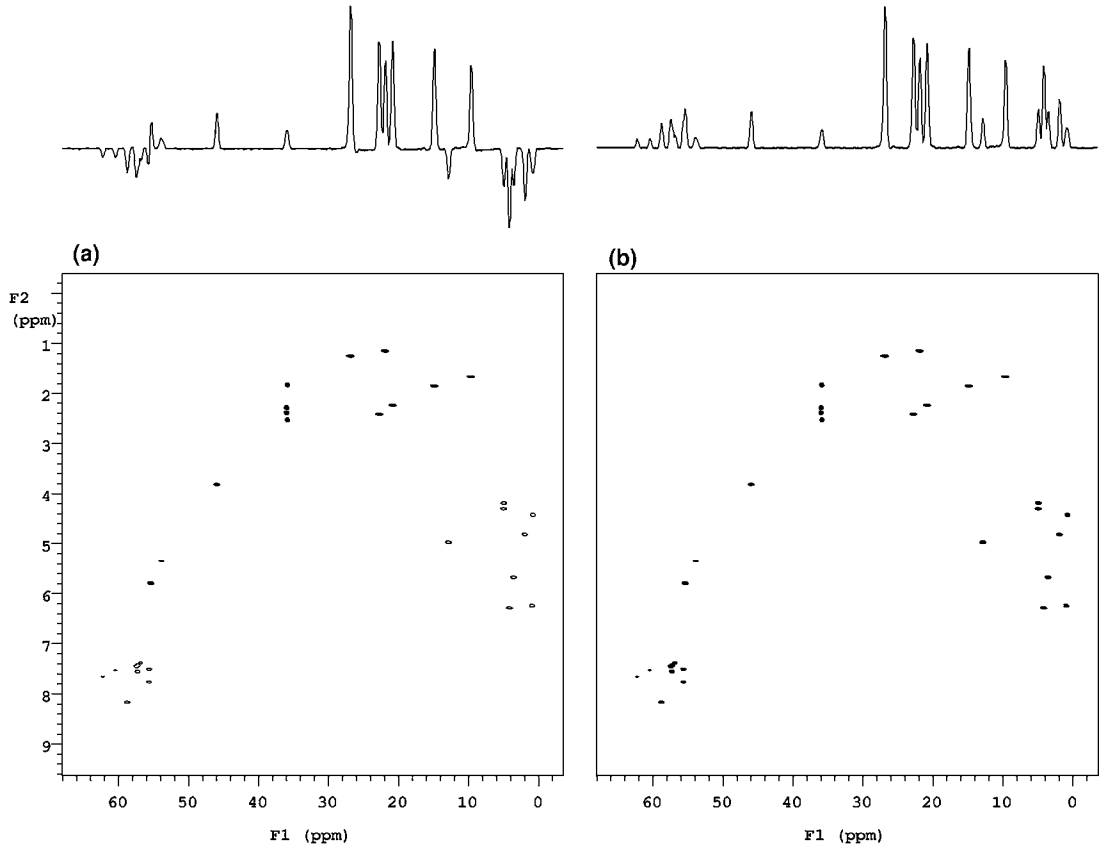

FIG. 4. IMPRESS-gHSQC spectra (unedited) of Taxol in CD_2Cl_2 using the sequence in Fig. 1B. (a) $S_1 = S_2 = S_{xx}$, where S_{xx} is a caWURST pulse of 8.8-ms duration ($B_{1(\mathrm{rms})} = 0.809$ kHz) to achieve 9-kHz bandwidth refocusing at $+/-4.5$-kHz off-resonance frequencies. The nominal phase of the two waveforms are the same. (b) $S_1 = S_{xx}$ and $S_2 = S_{xy}$, where S_{xy} is same as S_{xx} except that the nominal phase of the two waveforms is orthogonal. The spectra were acquired with the ^{13}C carrier set at 68 ppm, but processed with a -4.5-kHz frequency shift in the t_1 interferogram prior to F_1 transformation. F_1 projection is shown as well.

Each of the two edited IMPRESS-gHSQC spectra plotted in Fig. 5a is equivalent to eight scans (four scans each from the two unedited spectra) per increment collected over twice the t_1 acquisition time compared to the gHSQC spectrum in Fig. 5b (also eight scans per increment). To explore whether the increased sensitivity and resolution are purely due to the doubling of the t_1 acquisition time (collected over the same total experiment time), we compared two gHSQC spectra of strychnine in Fig. 7. These plots are expansions from spectra collected under identical total experiment time. The plots on the left (Figs. 7a and 7c) were from a data set collected over 512 t_1 increment data with four scans per increment. The plots on the right (Figs. 7b and 7d) were from a data set collected over 256 t_1 increment data with eight scans per increment. These expansions and projections were plotted with the vertical scaling factor adjusted such that the average (from four F_2 traces with no cross peaks) measured noise is the same in both spectra. While the resolution in the "4-512 scans-increment" spectrum is clearly higher, the sensitivity (peak height) is at best comparable to the "8-256 scans-increment" spectrum. In general, we find that increasing the number of t_1 increments at the expense of number of scans per increment typically results in poorer sensitivity, albeit increased F_1 resolution, and the comparison presented here is a best case scenario. Thus, the increased sensitivity in the IMPRESS-gHSQC experiment compared to the gHSQC experiment is clearly due to phase-encoded sampling (thus retaining the time averaging effect of eight scans per increment) and increased t_1 acquisition time (thus decreasing the linewidth along the F_1 dimension).

EXPERIMENTAL

All spectra were recorded at 25°C on a Varian UnityINOVA 500- or 300-MHz NMR spectrometer equipped with a programmable pulse modulator in the proton channel and a gradient accessory and using a $^1H\{X\}$ indirect detection probe. The band-selective π pulses (S_1 and S_2) in the DPFGSE are caWURST 180° pulses with appropriate phase modulation(s) to shift the centers of the refocusing profiles to the required offsets as noted in the figure legends. All shaped pulses were generated using Pandora's Box pulse shaping program (*26*) available in Varian NMR software. The gradients are rectangular shaped. All

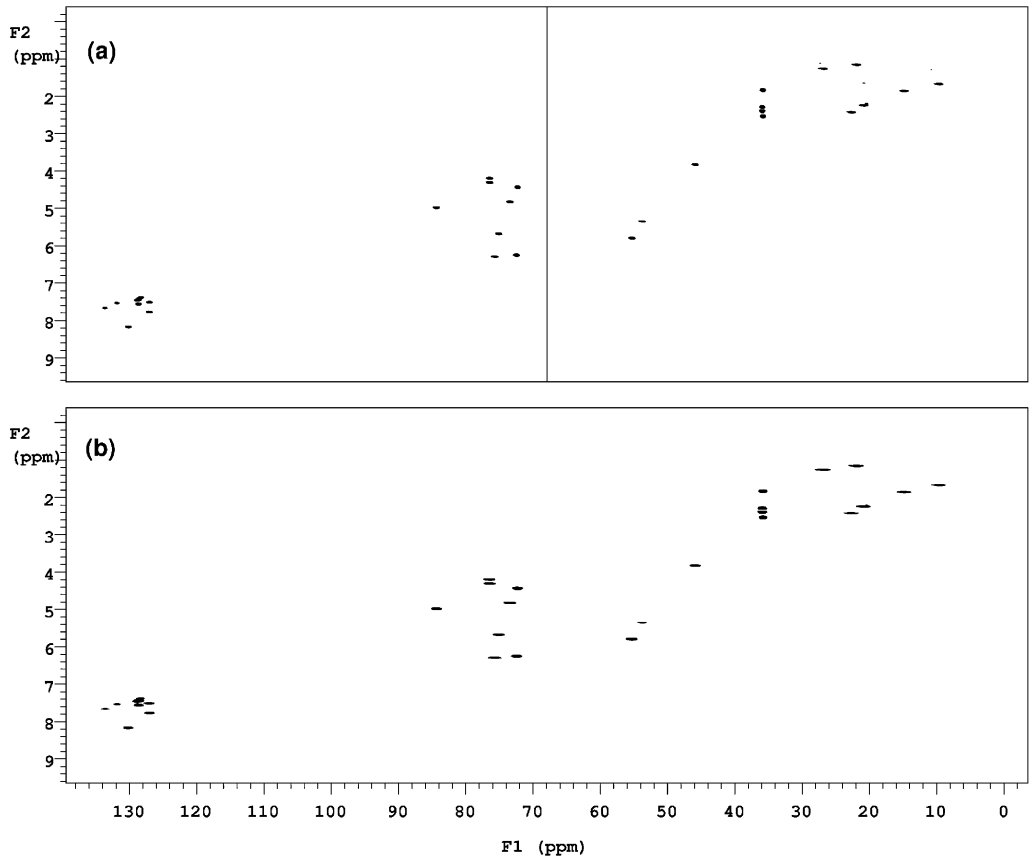

FIG. 5. Comparison of (a) edited IMPRESS-gHSQC and (b) nonselective gHSQC spectra of Taxol in CD_2Cl_2. The downfield half of spectrum a is obtained by adding the two spectra in Figs. 4a and 4b, while the upfield half is obtained by subtracting the two spectra in Figs. 4a and 4b. The addition and subtraction were done during the construction of t_1 interferogram. Frequency shifts of −4.5 and +4.5 kHz were applied to the t_1 interferograms prior to F_1 transformation to generate the downfield and upfield halves, respectively.

spectra were collected with the τ delay set to 1.67 ms (optimized for 150-Hz coupling), θ set to 0° pulse, and the Δ delay set to minimum length to accommodate the G5 gradient pulse, gradient recovery delay (500 μs), and the RF pulse. The typical ^{1}H 90° pulse width is 6 μs and nonselective ^{13}C 90° pulse width is 14 μs. All 2D data were processed with an unshifted gaussian window function in both F_1 and F_2 dimensions prior to Fourier transformation. To minimize the effect of postacquisition processing tools on the observed sensitivity or resolution, all spectra were processed without any linear prediction in either dimension. The editing was done by appropriate addition or subtraction of the data sets during the construction of the t_1 interferogram prior to F_1 transformation.

The DPFGSE profiles in Figs. 2a–2c were generated using a sample of D_2O, doped with $GdCl_3$ (linewidth of the residual HDO resonance is ∼2 Hz), and represent a sum of 101 scans each. The spectra were processed with 10-Hz exponential line broadening prior to Fourier transformation. The carrier frequency was shifted in between scans from +10 to −10 kHz (with respect to the on-resonance frequency of HDO) in steps of 200 Hz. The band-selective pulses S_1 and S_2 are either 8-ms (Fig. 2a) or 16-ms (Figs. 2b and 2c) caWURST shapes ($B_{1(\mathrm{rms})} =$ 0.893 and 631 kHz, respectively) to achieve 10-kHz refocusing on resonance (Fig. 2a) or 5-kHz refocusing at +/−2.5-kHz offresonance (Figs. 2b and 2c).

The nonselective and band-selective gHSQC spectra of strychnine in Fig. 3 were run using a sample of 10 mg/ml solution in $CDCl_3$ at 500 MHz proton observe frequency. The band-selective pulses S_1 and S_2 are 8.89-ms caWURST shapes ($B_{1(\mathrm{rms})} = 0.804$ kHz) to achieve 8.9-kHz refocusing. While the nonselective spectrum (Fig. 3a) was obtained using a ^{13}C spectral width of 17.8 kHz (142 ppm) centered around 71 ppm, the band-selective spectra in Fig. 3b and 3c were obtained using a ^{13}C spectral width of 8.9 kHz (71 ppm) each centered at 35.5 and 106.5 ppm, respectively. Eight scans of 2048 complex points were collected for each of the 200 t_1 increments. A recovery delay of 1 s was used prior to each scan and the total acquisition time for each of the three spectra was 1 h. The spectra were transformed after zero-filling to 2048 × 2048 complex points.

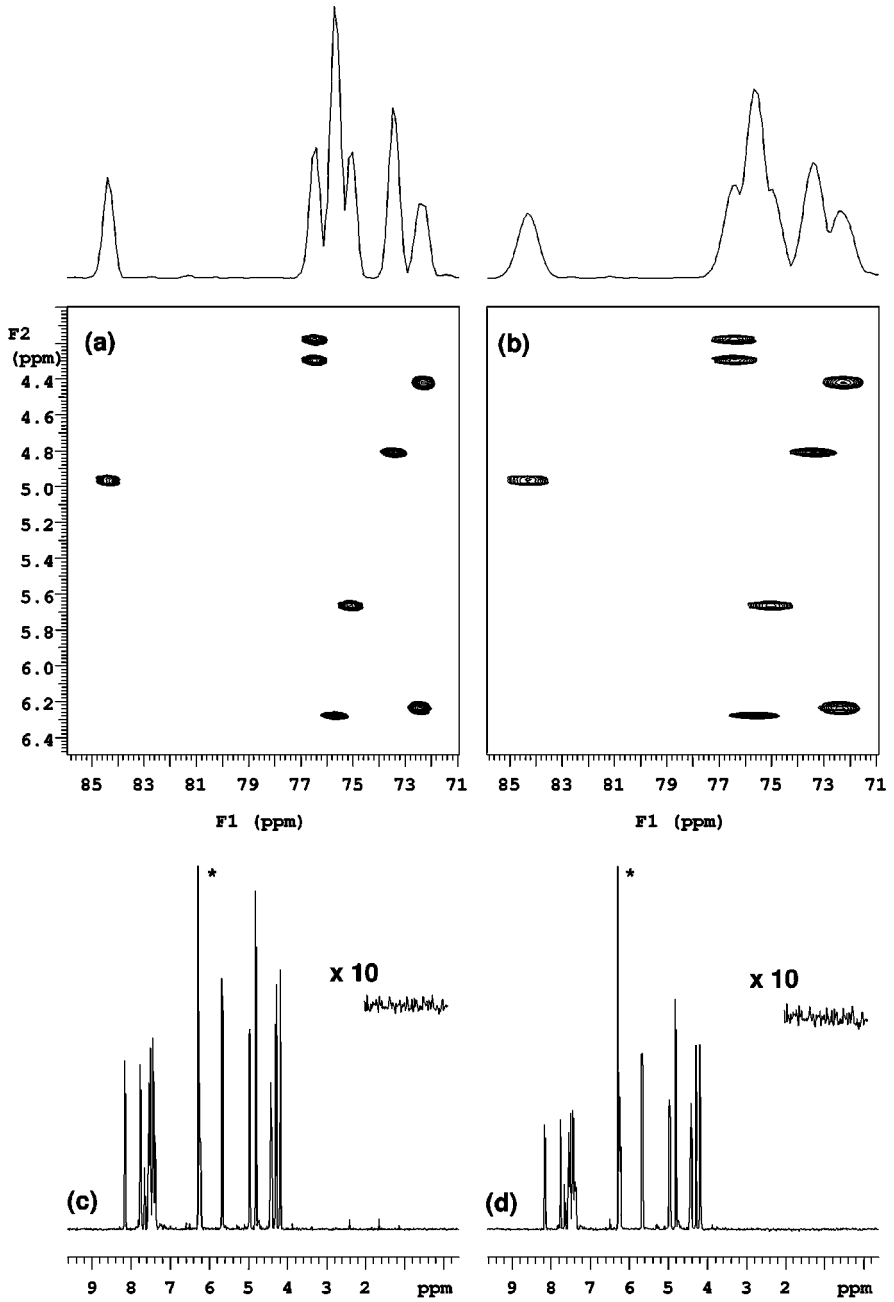

FIG. 6. Comparison of edited IMPRESS-gHSQC and nonselective gHSQC spectra of Taxol in CD_2Cl_2. (a) 2D expansion and F_1 projection of the IMPRESS-gHSQC; (b) 2D expansion and F_1 projection of the gHSQC; (c) F_2 projection of the "downfield" half of IMPRESS-gHSQC; and (d) F_2 projection of the "downfield" half of gHSQC. The peak marked with (*) is truncated in the plot. A 1-ppm noise expansion is shown as an inset plot.

The nonselective gHSQC spectra of strychnine in Fig. 7 were obtained using a sample of 10 mg/ml solution in CDC_3, at 300 MHz proton observe frequency. The spectra were obtained using a ^{13}C spectral width of 13 kHz centered at 80 ppm. The spectrum in Fig. 7a was collected over eight scans of 2048 complex points for each of the 256 t_1 increments. The spectrum in Fig. 7b was collected over four scans of 2048 complex points for each of the 512 t_1 increments. A recovery delay of 1 s was used prior to each scan and the total acquisition time was 1.5 h. The spectra were transformed after zero-filling to 2048 $\times$ 2048 complex points.

The spectra of Taxol in Figs. 4–6 were obtained using a sample of 10 mg/ml solution in CD_2Cl_2 at 500 MHz proton observe frequency. The IMPRESS-gHSQC spectra were obtained with a ^{13}C spectral width of 9 kHz and four scans of 2048 complex points over 180 t_1 increments. The

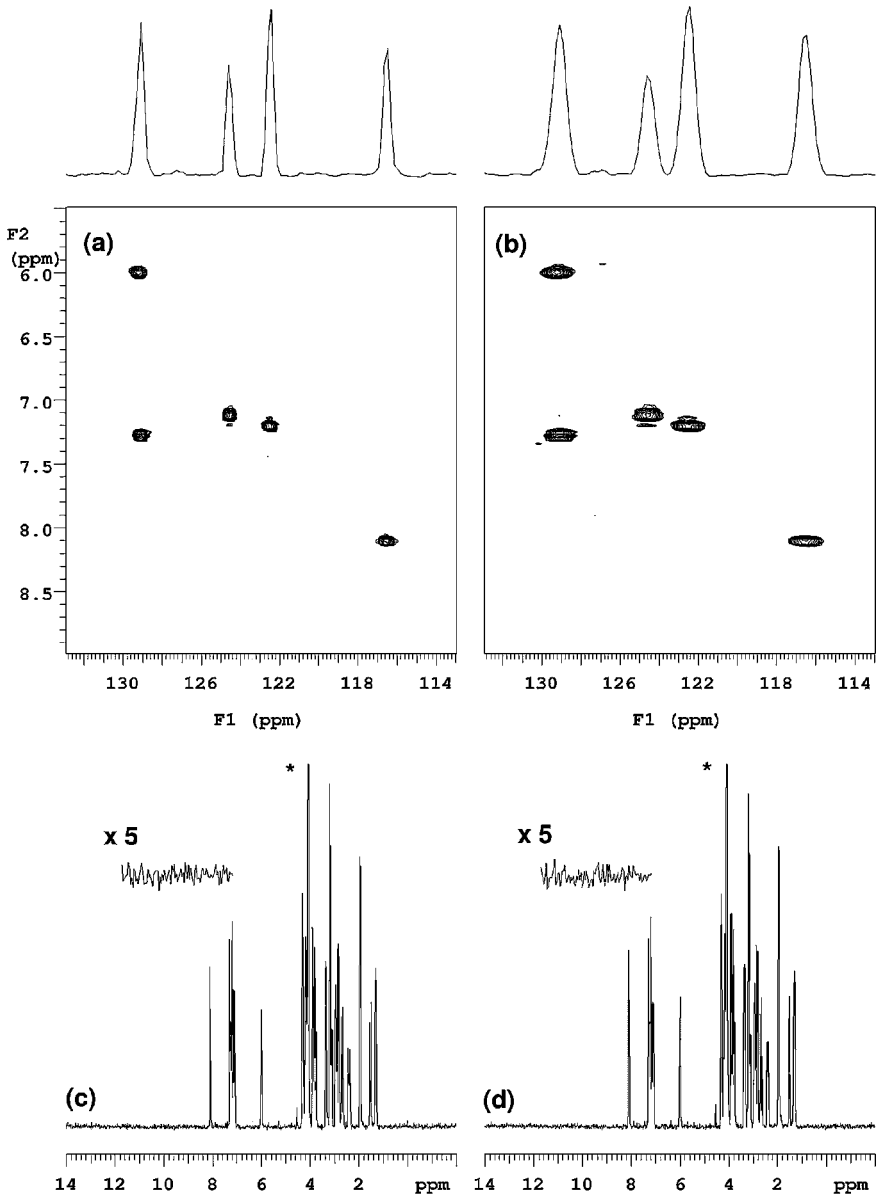

FIG. 7. Comparison of gHSQC spectra of strychnine in $CDCl_3$. (a,c) Four scans for each of the 512 t_1 increments; (b,d) Eight scans for each of the 256 t_1 increments. (a) 2D expansion and F_1 projection of the "4-512 scans-increment" gHSQC; (b) 2D expansion and F_1 projection of the "8-256 scans-increment" gHSQC; (c and d) F_2 projections. The peak marked with (*) is truncated in the plot. A 1-ppm noise expansion is shown as an inset plot.

band-selective pulses S_1 and S_2 in IMPRESS-gHSQC spectra are 8.8-ms caWURST shapes ($B_{1(\mathrm{rms})} = 0.804$ kHz) to achieve 9-kHz refocusing. A recovery delay of 1 s was used prior to each scan and the total acquisition time was 1 h. The spectra were transformed after zero-filling to 2048×1024 complex points. The gHSQC spectrum of Taxol was obtained under similar conditions as the IMPRESS-gHSQC spectra except for a ^{13}C spectral width of 18 kHz and eight scans per increments. The gHSQC spectra were transformed after zero-filling to 2048×2048 complex points. The ^{13}C carrier was set at 68 ppm in both cases.

CONCLUSION

The combination of excitation sculpting and phase encoding, as shown in the IMPRESS-gHSQC sequence in this report, thus provides a way to exploit spectral folding to improve F_1 resolution without the associated spectral crowding. The increased F_1 resolution (line narrowing) results in an increased peak height and S/N over a nonselective gHSQC experiment. We are further exploring ways to extend this to multiband selected two-dimensional experiments. This technique does involve long refocusing pulses and thus suffers from signal loss due to relaxation

during these pulses. For small molecules this loss due to relaxation is more than compensated by the increase in peak height (sensitivity) due to peak narrowing. But, the sensitivity gain (due to line narrowing) is expected to be significantly compromised in larger molecules. While we used exclusively caWURST refocusing pulses, we also find that the use of hyperbolic secant (*27*) or other WURST pulses (*24*, *25*) gives comparable results. We did not explore other band-selective pulses in the quest to find shorter pulse lengths and at the same time retain the flatter excitation profile. Since this experiment involves symmetrically shifted pulses, minimal out-of-band (and transition band) perturbation is a critical characteristic in selecting the waveforms. Careful consideration must also be given in positioning the ^{13}C carrier frequency and in calibrating (or calculating, as in the present case) the exact 180° pulse widths of the band-selective pulses. Any error in the pulse widths will manifest itself in a wider notch at the center of the excitation bandwidth, thus suppressing carbons at or near the carrier frequency.

REFERENCES

1. J. Cavanaugh, J. P. Waltho, and J. Keeler, *J. Magn. Reson.* **74,** 386 (1987).
2. R. Bruschweiler, J. C. Madsen, C. Griesinger, O. W. Sorensen, and R. R. Ernst, *J. Magn. Reson.* **81,** 561 (1987).
3. S. Berger, *J. Magn. Reson.* **81,** 561 (1989).
4. H. Kessler, U. Anders, G. Gemmecker, and S. Steuernagel, *J. Magn. Reson.* **85,** 1 (1989).
5. W. Bermel, K. Wagner, and C. Griesinger, *J. Magn. Reson.* **83,** 223 (1989).
6. L. Emsley, P. Huber, and G. Bodenhausen, *Angew. Chem., Int. Ed. Engl.* **29,** 517 (1990).
7. H. Kessler, S. Mronga, and G. Gemmecker, *Magn. Reson. Chem.* **29,** 527 (1991).
8. V. V. Krishnamurthy, *Magn. Reson. Chem.* **35,** 9 (1997).
9. C. Gaillet, C. Lequart, P. Debeire, and J.-M. Nuzillard, *J. Magn. Reson.* **139,** 454 (1999).
10. U. Eggenberger, P. Pfandler, and G. Bodenhausen, *J. Magn. Reson.* **77,** 192 (1988).
11. J. Hadamard, *Bull. Sci. Math.* **17,** 240 (1893).
12. R. Kaiser, *J. Magn. Reson.* **15,** 44 (1974).
13. R. Freeman and V. Blechta, *Chem. Phys. Lett.* **215,** 341 (1993).
14. V. Blechta, F. del Rio-Portilla, and R. Freeman, *Magn. Reson. Chem.* **32,** 134 (1994).
15. K. Scott, J. Stonehouse, J. Keeler, T. L. Hwang, and A. J. Shaka, *J. Am. Chem. Soc.* **117,** 4199 (1995).
16. V. V. Krishnamurthy, *J. Magn. Reson. A* **121,** 33 (1996).
17. V. V. Krishnamurthy, *J. Magn. Reson. B* **112,** 75 (1996).
18. V. V. Krishnamurthy, *J. Magn. Reson. B* **113,** 46 (1996).
19. Q. N. Van and A. J. Shaka, *J. Magn. Reson.* **132,** 154 (1998), and references therein.
20. K. Krishnamurthy, *J. Magn. Reson.*, in press.
21. S. L. Patt, *J. Magn. Reson.* **96,** 94 (1992).
22. For convenience, in this discussion, nominal phase is defined as the "end phase" of the individual waveforms that are being added to generate the multiple-frequency selected pulse. For refocusing (such as S_1 and S_2, in this case) the relative phase of two waveforms should be ideally defined at the midpoint of the pulse. However, we find that when used in a DPFGSE train, shapes with multiple waveforms and their relative phase defined at the beginning, middle, or end of the pulse produce the same result.
23. E. Kupče and R. Freeman, *J. Magn. Reson. A* **115,** 273 (1995).
24. E. Kupče and R. Freeman, *J. Magn. Reson. A* **118,** 299 (1996).
25. A. Tannus and M. Garwood, *J. Magn. Reson. A* **120,** 133 (1996).
26. E. Kupče and R. Freeman, *J. Magn. Reson. A* **105,** 234 (1993).
27. M. S. Silver, *J. Magn. Reson.* **59,** 347 (1984).